Journal of Theoretical and Applied Vibration and Acoustics 9(2) 39-53 (2023)

I S A V

Journal of Theoretical and Applied

Vibration and Acoustics

journal homepage: http://tava.isav.ir

Investigating the vibration of cracked micro-cantilever beam with concentrated mass and rotary inertia based on MCST

Hamed Petoft[a], **Abbas Rahi** [b,*]

[a]*Ph.D. Candidate, Faculty of Mechanical & Energy Engineering, Shahid Beheshti University, Tehran, Iran*

[b]*Associate Professor, Faculty of Mechanical & Energy Engineering, Shahid Beheshti University, Tehran, Iran*

ARTICLE INFO

Article history:
Received 14 February 2023

Received in revised form
5 June 2023

Accepted 23 October 2023

Available online 1 November 2023

Keywords:
Crack,

Micro-cantilever,

Beam,

MCST,

Mass ratio,

Inertia,

Natural frequency.

ABSTRACT

The current paper proposes the vibrational behavior of a cracked micro-cantilever Euler-Bernoulli beam with a concentrated mass and its moment of inertia at the free-end boundary condition based on the Modified Couple Stress Theory (MCST). We model the open-edge crack and calculate its stiffness. We also consider The Stress Intensity Factor (SIF). Using Hamilton's principle, the associated boundary conditions followed by the system's dynamic equations are derived based on MCST. Afterward, the natural frequencies of the cracked micro-cantilever beam are semi-analytically determined. In the numerical results, we obtain the first three natural frequencies of the system versus various parameters containing the crack depth and location changes and the material length scale parameter with the different mass ratios. The results are verified with similar previous research. The calculated results indicate that increasing the crack depth, approaching the crack location to the concentrated mass and the node points, and increasing the mass ratio cause a decrease in frequencies. However, increasing the material length scale parameter causes an increase in the natural frequencies due to raising the total strain energy of the system.

* Corresponding author:
E-mail address: a_rahi@sbu.ac.ir (A. Rahi)

http://dx.doi.org/10.22064/tava.2023.556982.1208

1. Introduction

Nowadays, the design of small-size structures has become increasingly important with the development of science and technology. Micro-beams, especially microcantilever beams are the fundamental components commonly used in Micro-Electro-Mechanical Systems (MEMS) such as microswitches and micro piezo-electric sensors [1-5]. Size-dependent theories are discussed in much-conducted research on micro-beams. Among them, Modified Couple Stress Theory (MCST) and Modified Strain Gradient Theory (MSGT) [6-10] are the most important. Wang et al. [3] used experimental experiments to show the flow rate sensitivity of an airflow sensor with a free-standing micro-cantilever as a MEMS-based structure. Chen and Zheng [6] investigated the static bending of an Euler-Bernoulli micro-beam with a surface-mounted zero-one polarized actuator with four different boundary conditions. They used MCST to capture size dependency and analytically calculated the maximum deflection of the beam in various boundary conditions. Joseph et al. [11] proposed a double micro-cantilever beam assuming surface effects and using Strain Gradient Theory to investigate the size-dependent effect and Stress-Intensity-Factors (SIF). Shafiei et al. [12] have presented a rotary tapered micro-cantilever beam and analyzed the first two frequencies with different values of the system design variables based on MCST. Using the Euler-Bernoulli theory for the simply-supported and cantilever beam, Kong et al. [13] analyzed the size dependency effect of the microbeam on the system's frequencies, and they analytically solved the problem using MCST. Park and Gao [14] also used MCST with Euler-Bernoulli's theory for bending a cantilever beam. Zhang et al. [4] obtained the dynamic equations of a micro-cantilever beam with a piezo-electric actuator and proposed an adaptive linear controller for the system. Taati and Sina [15] studied the static tensile behavior of an electrostatically actuated functionally graded (FG) micro-cantilever beam mounting on an elastic substrate using the MSGT.

Another interesting topic for researchers is the existence of faults in structures. Cracks are the most common damage to a component, especially in small sizes. In addition to crack detection [16-19], assumed as a crucial subject in research, crack modeling is also important to investigate its effect on the vibration behavior of systems. Often, in much scientific documentation, the crack is modeled as a spring with torsional stiffness, and its influence is studied on the natural frequencies of systems and examined component's life. Nakhaei et al. [20] proposed a cracked beam with two different circulars and the V-shape models for the breathing crack. Afterward, they investigated the influence of the crack parameters containing depth, shape, and location on the natural frequency. Fu et al. [21] assumed a simply-supported cracked beam with two different T-shapes and rectangular cross-sectional area and considered a nonlinear stress distribution model close to the crack in the system. Then, they presented an estimation for local and global stiffness. Zai et al. [22] studied the structural optimization of a cantilever beam with a midpoint load and optimized the geometry to minimize its final volume to obtain the minimum weight using analytical and Finite Element (FE) methods. They also calculated the first three natural frequencies of the cantilever beam without the midpoint load. Then, they compared the results with FEM. Khorshidi and Shariati [23] investigated a cracked Nano-beam with the Timoshenko model and assumed the axial force and bending moment with their couple effects. Kutukova et al. [24] used a micro-Double Cantilever Beam (micro-DCB) experimental test with an X-ray and the 3D structures microscope to study crack propagation in materials and analyze the fracture behavior of composite bulk materials. Joseph et al. [25] analytically researched the fracture behavior of a flexoelectric double cantilever beam (DCB) using SGT (or Strain Gradient Theory) and then presented numerical results. Akbas [26] considered an FG-cracked microcantilever beam with the Euler-

Bernoulli model and showed the crack parameters' effect, including the location and depth, on the system vibration behavior based on MCST. Akbas [27] also introduced a cracked Nano-cantilever circular beam under an external dynamic centralized force using MCST with Timoshenko beam theory and considering structural damping effect with the Kelvin–Voigt model. Rajasekaran and Khaniki [28] investigated the influence of Bi-Directional Functionally Graded (BDFG) cracked beams on the system's lateral vibration with two different boundary conditions containing cantilever and simply supported. Behera et al. [29] proposed a cracked cantilever beam and examined the effect of crack incline on the first three mode shapes. Shoaib et al. [30] assumed a piezoelectric cantilever MEMS sensor and analyzed the influence of the crack location on the displacement and resonance frequency without considering the size effect. Rahi [31] assumed a cracked simply-supported micro-beam using MCST and presented various models for Stress Intensity Factor (SIF). He analyzed the influence of the crack depth ratio η, the crack location L_C, and material-length-scale-parameter l on the crack equivalent torsional stiffness and the beam's first two natural frequencies. Rahi and Petoft [32] also analyzed the free vibration of a micro-beam with multiple cracks with the MCST model. They assumed an Euler-Bernoulli multi-crack micro-beam with simply-supported boundary conditions. They also provided a general solution for determining the equations of micro-beam boundary conditions with any desired number of cracks. Finally, they numerically investigated the effect of two cracks' existence on the first three natural frequencies. Laura et al. [33] analyzed the free vibration of a clamped-free (cantilever) Euler-Bernoulli beam with a concentrated mass at the beam's free end. They analytically calculated the eigenvalues (frequencies) as well as the mode shapes of the system. Then, they defined a mass ratio coefficient (the ratio of the concentrated mass to the beam's overall mass) and analyzed changes in the beam mode shapes and eigenvalues with different mass ratios in the numerical results. Wu and Lin [34] also studied the free vibration of a uniform cantilever beam with multi-concentrated masses with semi-analytical and Transfer Matrix Methods (TMM). They derived the eigenvalue equation analytically by using the expansion theorem. Then, they numerically calculated the eigenvalues and eigenvectors and assumed a cantilever beam with a concentrated mass at the free end condition. Finally, they computed the system's natural frequencies with various mass ratios.

Although there is much research about presenting the dynamic models of cracked beams, further study and research is needed to predict the dynamic behavior of these systems, especially in small-size structures. This paper presents a cracked micro-cantilever beam with an equivalent concentrated mass and its moment of inertia. This problem with a small size structure, especially microscale, has not been studied yet. In addition, the research outcome could be a fruitful method to predict the vibrational characteristics of MEMS sensors having similar conditions to the present model, especially when there is a fault (crack) in the system. The system's natural frequencies are analytically determined. Finally, in the numerical results, the effect of the mass ratio (the ratio of the concentrated mass to the beam's total mass), crack-existence parameters, including location and depth, and the material length scale parameter are investigated on the system's first three natural frequencies.

2. Modeling and governing equations of the system

According to Fig. 1, a cracked micro-cantilever beam is assumed. The open edge crack has depth a and location L_c from the clamp end. Also, the crack is considered perpendicular to the micro-beam's neutral axis without propagating behavior. A concentrated mass M with an equivalent mass

moment of inertia I_M around the Y-axis is connected to the free end. The micro-beam has a rectangular cross-section, with width b, height h, and length L with the coordinate system $X-Y-Z$.

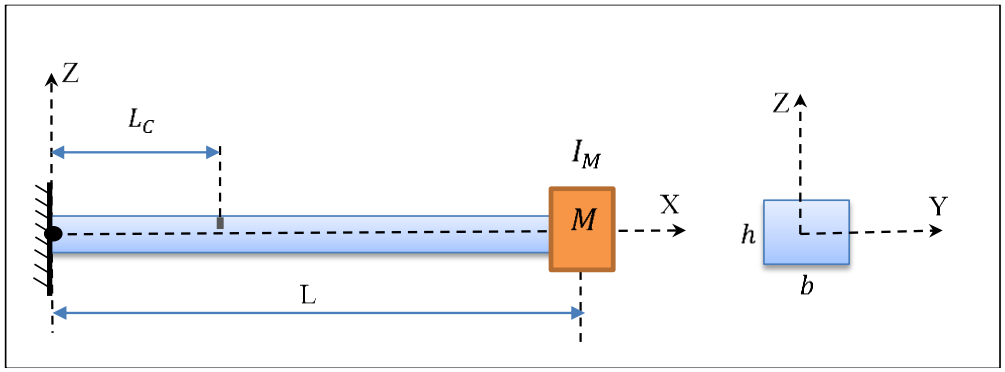

Fig. 1 Micro-cantilever beam with an open edge crack and concentrated mass and its equivalent moment of inertia at the end of the beam

Considering the crack as shown in Fig. 2, the lateral movement of the micro-beam can be divided into two segments ($w_1(x,t)$ and $w_2(x,t)$) with separate functions in terms of displacement and time. The crack is modeled with a torsional spring using a torsional stiffness. Thus, we divide the cracked micro-cantilever beam into two segments connected with a torsional spring at the location L_C (see Fig. 2). According to Fig. 2, the crack is modeled with a torsional spring with an equivalent stiffness K_t.

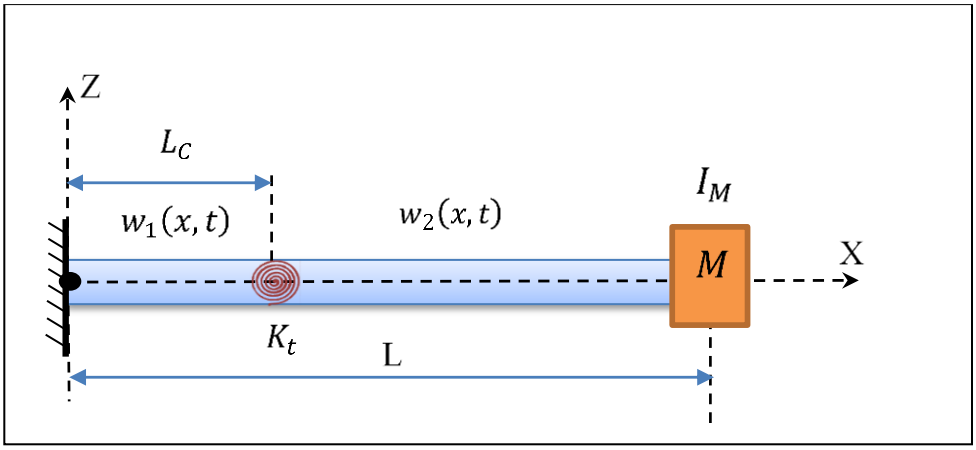

Fig. 2: Modeling of an open edge crack with a torsional spring

2.1. Mathematical model of crack stiffness

According to Rahi's research [31], the new models for calculating local stiffness are presented by considering the Stress Intensity Factor (SIF). Using model number 4, the equivalent torsional stiffness for the crack can be written as follows:

$$K_t = \frac{1}{\left[1+\frac{12}{(1+\vartheta)(1-\eta)^2}\left(\frac{l}{h}\right)^2\right]}\left[\frac{36EJ}{25\pi h(1-\vartheta^2)}\ \frac{(1-\eta)^3}{\eta^2(3-\eta)}\right] \quad (1)$$

where $\eta =$ a/h is a non-dimensional coefficient defined as the ratio of crack depth to the micro-beam height.

3. Determination of dynamic equations

The fundamental relationship to calculate the strain energy density (π_0) for elastic isotropic materials with the MCST model is presented as follows [31, 35]:

$$\pi_0 = \frac{1}{2}\sigma_{ij}\varepsilon_{ij} + \frac{1}{2}m_{ij}\,\chi^s_{ij} \tag{2}$$

where σ_{ij}, ε_{ij}, χ, and m_{ij} are, the stress tensor, symmetric curvature tensor, and the deviatory couple stress, respectively. These parameters in MCST are defined as follows:

$$\begin{gathered}\sigma_{ij} = 2\mu\varepsilon_{ij} + \lambda\varepsilon_{kk}\ ;\ \varepsilon_{ij} = \frac{1}{2}\left(u_{i,j} + u_{j,i}\right) \\ m_{ij} = 2\mu l^2\chi^s_{ij}\ ;\ \chi^s_{ij} = \frac{1}{2}\left(\theta_{i,j} + \theta_{j,i}\right)\ ;\ \theta_{i,j} = \frac{1}{2}\epsilon_{ijk}\,u_{i,j}\end{gathered} \tag{3}$$

In Eq. 3, θ_i, u_i, l, ϵ_{ijk} are components of the infinitesimal rotation vector, components of the displacement vector, material length scale parameter, and permutation symbol, respectively. Also, $\mu =$ E/2$(1+\vartheta)$ and $\lambda = E\vartheta/(1+\vartheta)(1-2\vartheta) = 2\mu\vartheta/(1-2\vartheta)$ are Lame's constants concerning Young's modulus E and Poisson's ratio ϑ.

Assuming the Euler-Bernoulli beam's model, the displacement vector in the micro-beam is presented as follows:

$$u_1 = -z\frac{\partial w(x,t)}{\partial x}\quad ;\quad u_2 = 0\quad ;\quad u_3 = w(x,t) \tag{4}$$

where $w(x,t)$ is the displacement of the micro-beam. Assuming small slope deformation in the micro-beam, the components of strain tensor ε and symmetric curvature tensor χ can be obtained as follows:

$$\begin{gathered}\varepsilon_{xx} = \frac{\partial u_1}{\partial x} = -z\frac{\partial^2 w}{\partial x^2}\ ;\ \varepsilon_{yy} = \varepsilon_{zz} = \varepsilon_{xy} = \varepsilon_{xz} = \varepsilon_{yz} = 0 \\ \chi^s_{12} = \chi^s_{21} = \frac{-1}{2}\frac{\partial^2 w}{\partial x^2}\ ;\ \chi^s_{11} = \chi^s_{22} = \chi^s_{23} = \chi^s_{32} = \chi^s_{13} = \chi^s_{31} = \chi^s_{33} = 0\end{gathered} \tag{5}$$

Now, putting Eqs. 3-5 in Eq. 2, the simplified strain energy density (π_0) can be obtained as follows:

$$\pi_0 = \frac{1}{2} E z^2 \left(\frac{\partial^2 w}{\partial x^2}\right)^2 + \frac{E l^2}{2(\vartheta + 1)} \left(\frac{\partial^2 w}{\partial x^2}\right)^2 \tag{6}$$

In this regard, the strain energy of each segment can be obtained by multiplying strain energy density by the cross-sectional area of the beam as follows:

$$\begin{gathered} \pi_{0A} = \int_A \pi_0 \, dA = \frac{1}{2} E \left(\frac{\partial^2 w}{\partial x^2}\right)^2 \int_A z^2 dA + \frac{El^2}{2(\vartheta + 1)} \left(\frac{\partial^2 w}{\partial x^2}\right)^2 \int_A dA \\ \pi_{0A} = \frac{1}{2} EJ \left(\frac{\partial^2 w}{\partial x^2}\right)^2 + \frac{El^2}{2(\vartheta + 1)} A \left(\frac{\partial^2 w}{\partial x^2}\right)^2 \end{gathered} \tag{7}$$

where $A = \int_A dA$ and $J = \int_A z^2 \, dA$ indicate the micro-beam cross-section area and moment of inertia, respectively. Considering the rectangular cross-section for the beam, $A = bh$ and $J = bh^3/12 = Ah^2/12$, thus $A = 12J/h^2$. By putting$A = 12J/h^2$ in Eq. 7 and integrating the beam's length element, the total strain energy (π_s) of the micro-beam is calculated as follows:

$$\pi_s = \int_L \pi_{0A} \, dx = \frac{1}{2} EJ \int_0^L \left(\frac{\partial^2 w}{\partial x^2}\right)^2 dx + \frac{1}{2} \frac{12EJ}{1 + \vartheta} \left(\frac{l}{h}\right)^2 \int_0^L \left(\frac{\partial^2 w}{\partial x^2}\right)^2 dx \tag{8}$$

The system's kinetic energy T is written as follows:

$$T = \frac{\rho}{2} \int_0^L [A \dot{w}^2] \, dx \tag{9}$$

where ρ is the density of the micro-beam.

In MCST, the material-length-scale-parameter (l) as the fundamental parameter in this method is used to consider the size dependency of the material in small-size (micro and nano) structures. According to Eq. 8, it is also clear that there is another term in addition to the total bending moment, which is dependent on the material-length-scale-parameter (l) to calculate the beam's total strain energy (π_s).

Based on Hamilton's principle, one may write:

$$\int_{t_1}^{t_2} \delta(T - \pi + W) \, dt = 0 \tag{10}$$

By substituting the Eqs. 8-9 into Eq. 10, and after simplifying the equations using variation calculus, the dynamic relation of the micro-beam is derived as follows:

$$S \frac{\partial^4 w}{\partial x^4} + \rho A \ddot{w} = 0 \tag{11}$$

where

$$S = EJ \left[1 + \frac{12}{1 + \vartheta} \left(\frac{l}{h}\right)^2\right] \tag{12}$$

The solution of Eq. 11 is obtained as follows using the separation of variables method:

$$w(x,t) = W(x).\{Acos(\omega t) + Bsin(\omega t)\} \tag{13}$$

where A and B are constant coefficients. By putting Eq. 13 into Eq. 11 and applying some simplifications, we have:

$$\frac{d^4W}{dx^4} - \beta^4 W(x) = 0$$
$$\beta^4 = \frac{\rho A \omega^2}{S} \;\rightarrow\; \omega^2 = \frac{\beta^4}{\rho A} S \tag{14}$$

where ω is natural frequency, ρ is the density of the micro-beam, and A is the cross-section of the micro-beam.

By solving Eq. 14, the general solution for each segment is obtained as follows:

$$\mathrm{W(x)} = \mathrm{C_1}\sin(\beta \mathrm{x}) + \mathrm{C_2}\cos(\beta \mathrm{x}) + \mathrm{C_3}\sinh(\beta \mathrm{x}) + \mathrm{C_4}\cosh(\beta \mathrm{x}) \tag{15}$$

where C_i , $(i = 1, 2, 3, 4)$ are constants.

Eq. 15 can be used for every segment and therefore, the dynamic equations of the two segments, respectively, are written as follows:

$$\mathrm{W_1(x)} = \tilde{\mathrm{C}}_1\sin(\beta \mathrm{x}) + \tilde{\mathrm{C}}_2\cos(\beta \mathrm{x}) + \tilde{\mathrm{C}}_3\sinh(\beta \mathrm{x}) + \tilde{\mathrm{C}}_4\cosh(\beta \mathrm{x})\,;\ 0 \le \mathrm{x} \le \mathrm{L_C}$$
$$W_2(x) = \tilde{C}_5\sin(\beta x) + \tilde{C}_6\cos(\beta x) + \tilde{C}_7\sinh(\beta x) + \tilde{C}_8\cosh(\beta x)\,;\ L_C \le x \le L \tag{16}$$

where $\tilde{C}_1$ to $\tilde{C}_8$ are constants. By assuming L_C as the crack location, the governing eight boundary conditions for the system are expressed as follows:

$$w_1(0,t) = 0 \;\;;\;\; \frac{\partial w_1}{\partial x}(0,t) = 0$$
$$S\frac{\partial^3 w_2(L,t)}{\partial x^3} = M\ddot{w}_2(L,t)$$
$$S\frac{\partial^2 w_2(L,t)}{\partial x^2} = I_M\frac{\partial \ddot{w}_2(L,t)}{\partial x}$$
$$w_1(L_c,t) = w_2(L_c,t) \tag{17}$$
$$\frac{\partial w_2}{\partial x}(L_c,t) - \frac{\partial w_1}{\partial x}(L_c,t) = \frac{\partial^2 w_1}{\partial x^2}(L_c,t) \times \frac{S}{K_t}$$
$$S\frac{\partial^2 w_1}{\partial x^2}(L_c,t) = S\frac{\partial^2 w_2}{\partial x^2}(L_c,t)$$
$$S\frac{\partial^3 w_1}{\partial x^3}(L_c,t) = S\frac{\partial^3 w_2}{\partial x^3}(L_c,t)$$

The obtained boundary conditions are described in the following sentences:

According to the system modeling as the cracked cantilever micro-beam with end concentrated mass and moment of inertia, the system has eight boundary conditions. For the clamp end, it is clear that the beam does not have any displacement or slope. Thus $w_1(0,t)=0$ and $\frac{\partial w_1}{\partial x}(0,t)=0$. For the free end with the concentrated mass (M) and inertia (I_M), we consider the equality of the bending moment of the beam with the angular acceleration of mass inertia and the shear force with the concentrated mass acceleration as $S\frac{\partial^2 w_2(L,t)}{\partial x^2}=I_M\frac{\partial \ddot{w}_2(L,t)}{\partial x}$ and $S\frac{\partial^3 w_2(L,t)}{\partial x^3}=M\ddot{w}_2(L,t)$. At the crack location, we similarly have the same boundary conditions as the equality of the bending moment, shear force, and displacement of two functions $W_1(x)$ and $W_2(x)$ as $S\frac{\partial^2 w_1}{\partial x^2}(L_c,t)=S\frac{\partial^2 w_2}{\partial x^2}(L_c,t)$, $S\frac{\partial^3 w_1}{\partial x^3}(L_c,t)=S\frac{\partial^3 w_2}{\partial x^3}(L_c,t)$, and $w_1(L_c,t)=w_2(L_c,t)$. The last one is defined at the crack location as the equality of the beam's bending moment with the crack's bending moment due to its equivalent torsional stiffness (K_t) as $K_t\theta=S\frac{\partial^2 w_1}{\partial x^2}(L_c,t)$ where $\theta=\frac{\partial w_2}{\partial x}(L_c,t)-\frac{\partial w_1}{\partial x}(L_c,t)$.

By replacing Eqs. 13-14 into Eq. 17, Eq. 18 can be rewritten as follows:

$$
\begin{gathered}
W_1(0)=0\ ;\quad \frac{dW_1}{dx}(0)=0\\
\frac{d^3W_2}{dx^3}(L)+\frac{M\beta^4}{\rho A}W_2(L)=0\\
\frac{d^2W_2}{dx^2}(L)+\frac{I_M\beta^4}{\rho A}\frac{dW_2}{dx}(L)=0\\
W_1(L_c)=W_2(L_c)\\
K_t\left(\frac{dW_2}{dx}(L_c)-\frac{dW_1}{dx}(L_c)\right)=S\frac{d^2W_1}{dx^2}(L_c)\\
S\frac{d^2W_1}{dx^2}(L_c)=S\frac{d^2W_2}{dx^2}(L_c)\\
S\frac{d^3W_1}{dx^3}(L_c)=S\frac{d^3W_2}{dx^3}(L_c)
\end{gathered}
\tag{18}
$$

where K_t is the crack equivalent local stiffness with the torsional spring model. By substituting Eq. 18 into Eq. 16, a set of 8 algebraic equations result in matrix form which is presented as follows:

$$[Q(i,j)]\{\tilde{C}_j\}=0\ ;\quad i,j=1,\qquad 2,\dots,8 \tag{19}$$

where the non-zero elements of the matrix $[Q]$ can be expressed as follows

$$Q(1,2) = 1 \; ; \quad Q\,(1,4) = 1$$

$$Q(2,1) = \beta; \; Q(2,3) = \beta$$

$$Q(3,5) = -\beta^3 cos(\beta L) + \frac{M\beta^4}{\rho A} sin(\beta L) \; ; \; Q(3,6) = \beta^3 sin(\beta L) + \frac{M\beta^4}{\rho A} cos(\beta L)$$

$$Q(3,7) = \beta^3 cosh(\beta L) + \frac{M\beta^4}{\rho A} sinh(\beta L) \; ; \; Q(3,8) = \beta^3 sinh(\beta L) + \frac{M\beta^4}{\rho A} cosh(\beta L)$$

$$Q(4,5) = -\beta^2 \, sin(\beta L) + \frac{I_M\beta^5}{\rho A} cos(\beta L) \; ; \; Q(4,6) = -\beta^2 \, cos(\beta L) - \frac{I_M\beta^5}{\rho A} sin(\beta L)$$

$$Q(4,7) = \beta^2 \, sinh(\beta L) + \frac{I_M\beta^5}{\rho A} cosh(\beta L); \; Q(4,8) = \beta^2 \, cosh(\beta L) + \frac{I_M\beta^5}{\rho A} sinh(\beta L)$$

$$Q(5,1) = sin(\beta L_c) \; ; \; Q(5,2) = cos(\beta L_c)$$

$$Q(5,3) = sinh(\beta L_c) \; ; \; Q(5,4) = cosh(\beta L_c)$$

$$Q(5,5) = -sin(\beta L_c) \; ; \; Q(5,6) = -cos(\beta L_c)$$

$$Q(5,7) = -sinh(\beta L_c) \; ; \; Q(5,8) = -cosh(\beta L_c)$$

$$Q(6,1) = \beta \cos(\beta L_c) - \frac{S\beta^2}{K_t} \sin(\beta L_c) \; ; \quad Q(6,2) = -\beta \sin(\beta L_c) - \frac{S\beta^2}{K_t} \cos(\beta L_c) \tag{20}$$

$$Q(6,3) = \beta \, cosh(\beta L_c) + \frac{S\beta^2}{K_t} sinh(\beta L_c) \; ; \; Q(6,4) = \beta \, sinh(\beta L_c) + \frac{S\beta^2}{K_t} cosh(\beta L_c)$$

$$Q(6,5) = -\beta \, cos(\beta L_c) \; ; \; Q(6,6) = \beta \, sin(\beta L_c)$$

$$Q(6,7) = -\beta \, cosh(\beta L_c) \; ; \; Q(6,8) = -\beta \, sinh(\beta L_c)$$

$$Q(7,1) = -\beta^2 sin(\beta L_c) \; ; \; Q(7,2) = -\beta^2 cos(\beta L_c)$$

$$Q(7,3) = \beta^2 sinh(\beta L_c) \; ; \; Q(7,4) = \beta^2 cosh(\beta L_c)$$

$$Q(7,5) = \beta^2 sin(\beta L_c) \; ; \; Q(7,6) = \beta^2 cos(\beta L_c)$$

$$Q(7,7) = -\beta^2 sinh(\beta L_c) \; ; \; Q(7,8) = -\beta^2 cosh(\beta L_c)$$

$$Q(8,1) = -\beta^3 cos(\beta L_c) \; ; \; Q(8,2) = \beta^3 sin(\beta L_c)$$

$$Q(8,3) = \beta^3 cosh(\beta L_c) \; ; \; Q(8,4) = \beta^3 sinh(\beta L_c)$$

$$Q(8,5) = \beta^3 cos(\beta L_c) \; ; \; Q(8,6) = -\beta^3 sin(\beta L_c)$$

$$Q(8,7) = -\beta^3 cosh(\beta L_c) \; ; \; Q(8,8) = -\beta^3 sinh(\beta L_c)$$

Considering the zero value for the determinant of the matrix $[Q]$ and solving Eq. 20 with respective to β, the natural frequencies can be calculated by the semi-analytical method.

4. Numerical results and discussion

In this section, we innovatively present the numerical results for a cracked micro-cantilever beam with different concentrated mass and rotary inertia values. The system has the following

mechanical properties [31]: Young modulus $\mathrm{E} = 1.44\ GPa$, Poison ratio $\vartheta = 0.38$, and density $\rho = 1220\,\frac{\mathrm{kg}}{\mathrm{m}^3}$. The micro-beam dimensions are the height $h = 20\ \mu m$, width $b = 2h$, $L = 20h$, the beam's moment of inertia $J = \frac{1}{12}bh^3$, and material length scale parameter $l = 0.5h$. In this regard, we can calculate the equivalent mass at the end of the cantilever. Hence, the R symbol is defined as a concentrated to the beam overall mass ratio. In this regard, we can calculate the equivalent mass at the end of the cantilever. Dimensions of the rectangular point mass are $a' = 100\ \mu m$, $b' = 100\ \mu m$. Therefore, the concentrated mass and its rotary moment of inertia at the clamped-end boundary condition are obtained as follows:

$$R = \frac{M}{m} \ \rightarrow \ M = mR = \rho ALR$$
$$I_M = \frac{1}{12}M(a'^2 + b'^2) + ML^2 \tag{21}$$

Considering these assumptions, the equations and the system's natural frequencies are determined numerically by defining the determinant of the matrix Q to zero. In this study, we investigate the variation of the first three natural frequencies by changing the crack parameters (including the crack depth ratio (η) and crack location (L_C)) and the mass ratio (R) as follows:

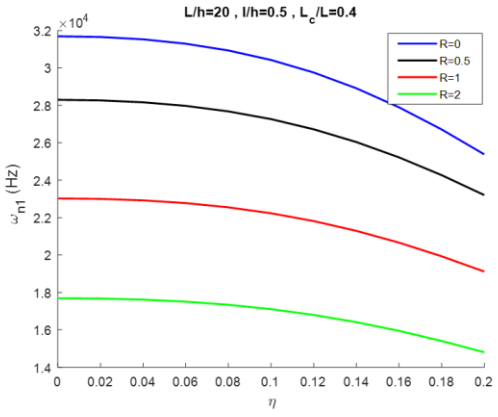

Fig. (3) The first natural frequency variation versus the crack depth ratio with different mass ratios(R)

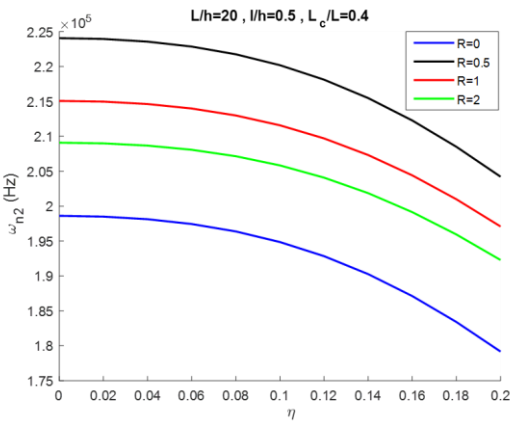

Fig. (4) The first natural frequency variation versus the crack depth ratio with different mass ratios(R)

According to Figs. 3-5, the first three natural frequencies of the system ($\omega_{n1}, \omega_{n2}, \omega_{n3}$) are plotted versus cracks depth ratio (η) with four different mass ratios ($R = 0,\ 0.5,\ 1, 2$); the location of the first crack is fixed at $\frac{L_C}{L} = 0.4$. The results show that the natural frequencies decrease by increasing the crack depth (η) and the mass ratio R. Additionally, in Figs. 6-8, the natural frequencies ($\omega_{n1}, \omega_{n2}, \omega_{n3}$) are obtained by changing the crack location ratio ($\frac{L_C}{L}$) with the same four different mass ratios again ($R = 0,\ 0.5,\ 1, 2$); However, the crack depth ratio is assumed constant with $\eta = 0.2$ this time.

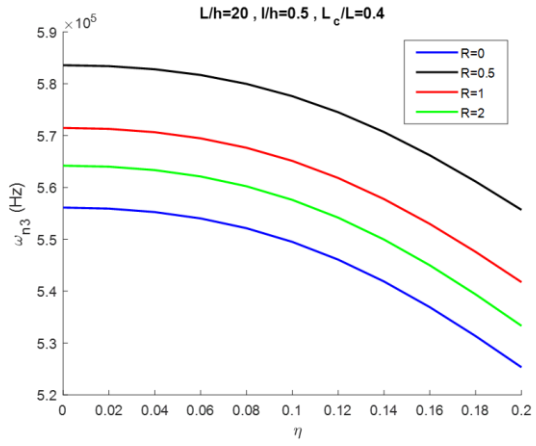

Fig. (5) The third natural frequency variation versus the crack depth ratio with different mass ratios(R)

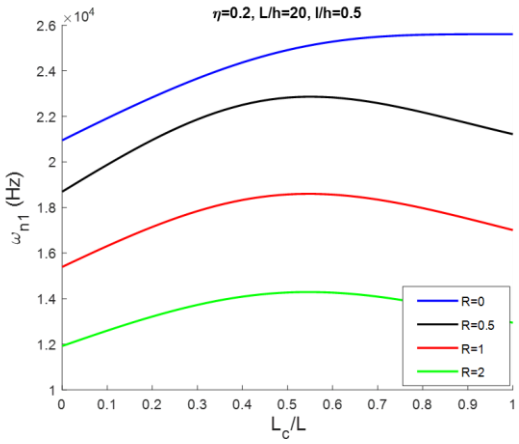

Fig. (6) the first natural frequency variation versus the crack location with different mass ratios(R)

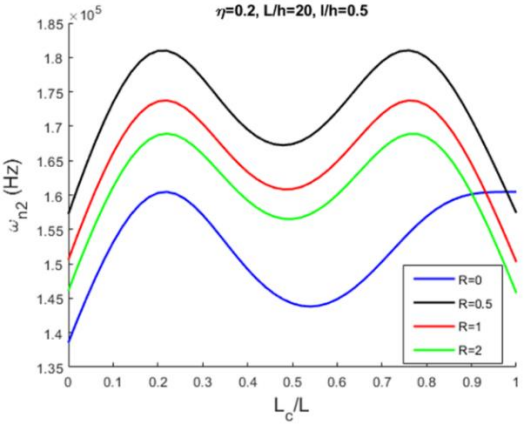

Fig. (7) the second natural frequency variation versus the crack location with different mass ratios(R)

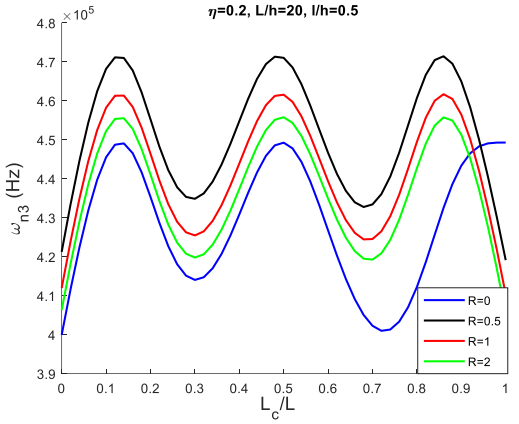

Fig. (8) The third natural frequency variation versus the crack location with four different mass ratios(R)

Increasing R means raising the concentrated mass (M) and the mass moment of inertia (I_M), according to Eq.21. The first natural frequency (ω_{n1}) is decreased by increasing R and followed by an increase in M and I_M (Figs.3&6). About the other natural frequencies (ω_{n2}, ω_{n3}), although increasing R causes a decrease in ω_{n2}, ω_{n3}, due to the existence of node points from the second frequency onwards, the frequencies are further than in the case of without concentrated mass and its inertia or $R = 0$ (Figs.4-5 & 7-8). Now, in the diagrams of the frequencies versus the crack position, according to Figs.6-8, it is clear that the frequency behavior increases harmonically and decreases relative to the crack position. The local minimum points imply the node points in the system. In the first frequency diagram, there isn't any local minimum point. So, the first frequency has no node point. In the second frequency diagram, there is one minimum point near $L_c/L = 0.5$. So, this is the node point of the system in the second mode. For the third frequency diagram, there are two local minimum points close to $L_c/L = 0.3$ and $L_c/L = 0.7$. They are the node points of the third mode frequency similarly. Moreover, the natural frequencies are minimum at both ends of the beam containing the first clamp condition and concentrated mass along with its moment of

inertia at the free end. Note, in the specific case of $R = 0$, the system is converted to the clamp-free condition that the frequency is the maximum value at the free end.

In another case, the material length scale parameter (l) is changed to analyze its effect on the natural frequencies. In this regard, we fix the crack depth and location at $\eta = 0.2$ and $\frac{L_c}{L} = 0.4$. Then, the material length scale parameter changes from 0 to $10\mu m$ with different mass ratios (R) again. The obtained results are shown as follows:

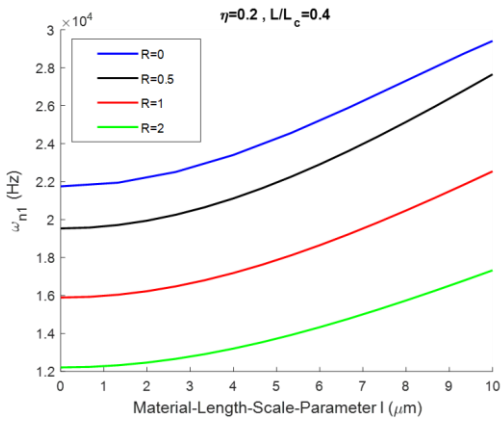

Fig. (9) The first natural frequency variation versus the material length scale parameter with different mass ratios

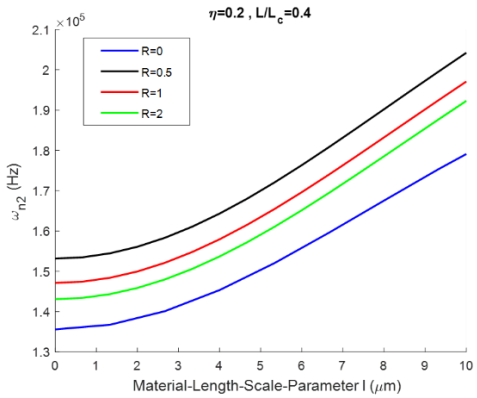

Fig. (10) The second natural frequency variation versus the material length scale parameter with different mass ratios

According to Figs. 9-11, increasing the material length scale parameter (l) causes an increase in all frequencies with the nonlinear behavior form. This issue occurs because of a rise in the system's total strain energy (π_s) by increasing the material length scale parameter (l) according to Eq. (8). The changing mass ratio (R) provides a similar effect on the frequencies, as expressed before.

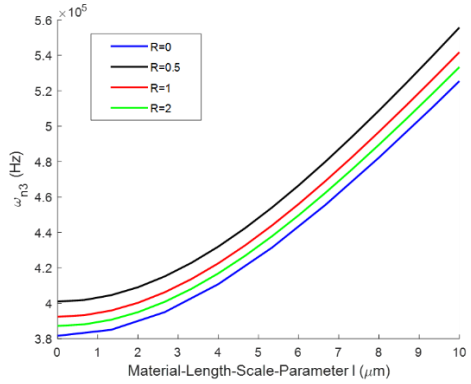

Fig. (11) The third natural frequency variation versus the material length scale parameter with different mass ratios

5. Case study verification

In a specific case, if the material length scale parameter is assumed to be insignificant or $l \approx 0$, the micro-beam is converted to a macro-state, and respectively by neglecting the effect of the crack and the concentrated mass with considering $\eta = 0$ and $R = 0$, the system converts to a simple

Euler-Bernoulli cantilever beam with a free end. Therefore, the natural frequencies of the clamp-free Euler-Bernoulli beam can be calculated as follows [36]:

$$\omega_n(Hz) = \left(\frac{1}{2\pi}\right)(\alpha_n)^2\left(\frac{EJ}{\rho AL^4}\right)^{\frac{1}{2}}; \quad (n = 1, 2, \dots) \tag{22}$$

The first three natural frequencies of the system are computed by replacing the mechanical properties of the beam as follows:

$$\begin{aligned}
\omega_{n1} &= \left(\frac{1}{2\pi}\right)(\alpha_1 = 1.875)^2\left(\frac{EJ}{\rho AL^4}\right)^{\frac{1}{2}} = 2.1935 * 10^4\ (Hz)\\
\omega_{n2} &= \left(\frac{1}{2\pi}\right)(\alpha_2 = 4.694)^2\left(\frac{EJ}{\rho AL^4}\right)^{\frac{1}{2}} = 1.3748 * 10^5\ (Hz)\\
\omega_{n3} &= \left(\frac{1}{2\pi}\right)(\alpha_3 = 7.855)^2\left(\frac{EJ}{\rho AL^4}\right)^{1/2} = 3.8498 * 10^5\ (Hz)
\end{aligned} \tag{23}$$

These analytical results equal the obtained frequencies of the present solving method in this specific case.

In another specific case, if the material length scale parameter and the crack effect are ignored anew (respectively, by substituting $l = 0$ and $\eta = 0$), the system will be simplified to a cantilever beam with a concentrated mass at the free end. It is similar to Laura et al.[33] work and the numerical case study of Wu and Lin [34]. For this reason, considering their numerical values for the beam mechanical properties, including $E = 30 * 10^6\ Psi$, the beam mass per unit length $m = 0.8891\ Ibm/inch$, the beam diameter $d = 2\ inch$, the beam length $L = 40\ inch$, and $R = 1$ without the mass moment of inertia ($I_M = 0$), along with considering $1\ in = 25.4\ mm$, $1\ lbm = 0.45\ kg$, $1\ lbf = 4.45\ N$, $1\ psi = 6894.76\frac{N}{m^2}$ as the units conversion factors, we compare the obtained numerical results of the present work with their similar research for calculating the first three natural frequencies of the beam as follows:

Table 1. Comparing numerical results of the present work for computing the first three natural frequencies of the cantilever beam along with a concentrated mass at the free end with other studies

Research	$\omega_{n1}\ (\frac{rad}{sec})$	$\omega_{n2}\ (\frac{rad}{sec})$	$\omega_{n3}\ (\frac{rad}{sec})$
Present	5.1305	53.4805	167.4843
Wu and Lin [34]	5.0111	52.2837	164.1022
Laura et al. [33]	5.0105	52.2007	163.7544
Difference with Wu and Lin [34] (%)	2.33	2.24	2.02
Difference with Laura et al. [33] (%)	2.34	2.39	2.23

According to Table. 1, it seems that the present numerical method results are approximately compatible with the results of other similar previous studies [33, 34].

6. Summary and conclusion

In this article, a cracked microcantilever beam is studied with a concentrated mass and its related moment of inertia at the beam's end based on MCST. Afterward, the effect of the mass ratio (R) and the crack parameters including the depth and the location, was investigated on the natural frequencies of the micro-cantilever beam. First, a non-propagated open-edge crack with a torsional spring based on MCST was considered. Then, the governing dynamic equations and the boundary conditions were derived using Hamilton's principle. The obtained equations were solved using the method of separation of the variables. Afterward, the first three natural frequencies of the system were semi-analytically calculated.

The numerical results showed that increasing the crack depth causes a decrease in natural frequencies remarkably with nonlinear behavior form. Additionally, every frequency is decreased by approaching the crack location to the concentrated mass and the node points. In this regard, the minimum local frequencies versus the crack location imply the node points of the system. Therefore, the system in the first natural frequency (first mode) has no node point, the second mode has a node point (close to $\frac{L_c}{L} = 0.5$), and the third mode has two node points (close to $\frac{L_c}{L} = 0.3, 0.7$). Also, based on the obtained results, by comparing different ratios of the concentrated mass to the beam's total mass, increasing the mass ratio (R) with increasing the mass moment of inertia causes a decrease in the frequencies. Finally, according to the results, increasing the material length scale parameter increases the frequencies nonlinearly due to raising the total strain energy of the system.

References

[1] R.A. Coutu, P.E. Kladitis, L.A. Starman, J.R. Reid, A comparison of micro-switch analytic, finite element, and experimental results, Sensors and Actuators A: Physical, 115 (2004) 252-258.
[2] V.R. Mamilla, K.S. Chakradhar, Micro Machining for Micro Electro Mechanical Systems (MEMS), Procedia Materials Science, 6 (2014) 1170-1177.
[3] C.-Y.L. Yu-Hsiang Wang, Che-Ming Chiang, A MEMS-based Air Flow Sensor with a Free-standing Microcantilever Structure, sensors, (2007).
[4] W. Zhang, G. Meng, H. Li, Adaptive vibration control of micro-cantilever beam with piezoelectric actuator in MEMS, The International Journal of Advanced Manufacturing Technology, 28 (2005) 321-327.
[5] M. Ghavami, S. Azizi, M.R. Ghazavi, On the dynamics of a capacitive electret-based micro-cantilever for energy harvesting, Energy, 153 (2018) 967-976.
[6] M. Chen, S. Zheng, Size-dependent static bending of a micro-beam with a surface-mounted 0–1 polarized PbLaZrTi actuator under various boundary conditions, Journal of Intelligent Material Systems and Structures, 28 (2017) 2920-2932.
[7] B. Akgöz, Ö. Civalek, Strain gradient elasticity and modified couple stress models for buckling analysis of axially loaded micro-scaled beams, International Journal of Engineering Science, 49 (2011) 1268-1280.
[8] A.C.M.C. F. Yang, D.C.C. Lam, P. Tong, Couple stress based strain gradient theory for elasticity, International Journal of Solids and Structures 39, 2731–2743, (2002).
[9] W.H.M. Christian Liebold, Applications of Strain Gradient Theories to the Size Effect in Submicro Structures incl. Experimental Analysis of Elastic Material Parameters, Bulletin of TICMI, Vol. 19, No. 1, 45–55, (2015).
[10] J. Fang, J. Gu, H. Wang, Size-dependent three-dimensional free vibration of rotating functionally graded microbeams based on a modified couple stress theory, International Journal of Mechanical Sciences, 136 (2018) 188-199.
[11] R.P. Joseph, Wang, B., Samali, B., Size-dependent stress intensity factors in a gradient elastic double cantilever beam with surface effects, Archive of Applied Mechanics, (2018).

[12] N. Shafiei, M. Kazemi, L. Fatahi, Transverse vibration of rotary tapered microbeam based on modified couple stress theory and generalized differential quadrature element method, Mechanics of Advanced Materials and Structures, 24 (2016) 240-252.
[13] S. Kong, S. Zhou, Z. Nie, K. Wang, The size-dependent natural frequency of Bernoulli–Euler micro-beams, International Journal of Engineering Science, 46 (2008) 427-437.
[14] X.-L.G. S. K. Park, A new Bernoulli-Euler beam model based on a modified couple stress theory, Journal of Micromechanics and Microengineering, Volume 16, Number 11, (2006).
[15] E. Taati, N. Sina, Static Pull-in Analysis of Electrostatically Actuated Functionally Graded Micro-Beams Based on the Modified Strain Gradient Theory, International Journal of Applied Mechanics, 10 (2018) 1850031.
[16] A. Khnaijar, R. Benamar, A new model for beam crack detection and localization using a discrete model, Engineering Structures, 150 (2017) 221-230.
[17] K.V. Nguyen, Q. Van Nguyen, Element stiffness index distribution method for multi-crack detection of a beam-like structure, Advances in Structural Engineering, 19 (2016) 1077-1091.
[18] H. Chouiyakh, L. Azrar, K. Alnefaie, O. Akourri, Vibration and multi-crack identification of Timoshenko beams under moving mass using the differential quadrature method, International Journal of Mechanical Sciences, 120 (2017) 1-11.
[19] K. Zhang, X. Yan, Multi-cracks identification method for cantilever beam structure with variable cross-sections based on measured natural frequency changes, Journal of Sound and Vibration, 387 (2017) 53-65.
[20] A. Mofid Nakhaei, M. Dardel, M. Hassan Ghasemi, Modeling and frequency analysis of beam with breathing crack, Archive of Applied Mechanics, (2018).
[21] C. Fu, Y. Wang, D. Tong, Stiffness Estimation of Cracked Beams Based on Nonlinear Stress Distributions Near the Crack, Mathematical Problems in Engineering, 2018 (2018) 1-12.
[22] B.A. Zai, M. Park, S.-C. Lim, J.-W. Lee, R.A. Sindhu, Structural Optimization of Cantilever Beam in Conjunction with Dynamic Analysis, in: Proceedings of the Computational Structural Engineering Institute Conference, Computational Structural Engineering Institute of Korea, 2008, pp. 397-401.
[23] M. Akbarzadeh Khorshidi, M. Shariati, A multi-spring model for buckling analysis of cracked Timoshenko nanobeams based on modified couple stress theory, Journal of Theoretical and Applied Mechanics, (2017) 1127.
[24] K. Kutukova, S. Niese, J. Gelb, R. Dauskardt, E. Zschech, A novel micro-double cantilever beam (micro-DCB) test in an X-ray microscope to study crack propagation in materials and structures, Materials Today Communications, 16 (2018) 293-299.
[25] R.P. Joseph, C. Zhang, B.L. Wang, B. Samali, Fracture analysis of flexoelectric double cantilever beams based on the strain gradient theory, Composite Structures, 202 (2018) 1322-1329.
[26] Ş.D. Akbaş, Free Vibration of Edge Cracked Functionally Graded Microscale Beams Based on the Modified Couple Stress Theory, International Journal of Structural Stability and Dynamics, 17 (2017) 1750033.
[27] Ş.D. Akbaş, Forced vibration analysis of cracked nanobeams, Journal of the Brazilian Society of Mechanical Sciences and Engineering, 40 (2018).
[28] S. Rajasekaran, H.B. Khaniki, Free vibration analysis of bi-directional functionally graded single/multi-cracked beams, International Journal of Mechanical Sciences, 144 (2018) 341-356.
[29] R.K. Behera, A. Pandey, D.R. Parhi, Numerical and Experimental Verification of a Method for Prognosis of Inclined Edge Crack in Cantilever Beam based on Synthesis of Mode Shapes, Procedia Technology, 14 (2014) 67-74.
[30] M. Shoaib, N.H. Hamid, M. Tariq Jan, N.B. Zain Ali, Effects of Crack Faults on the Dynamics of Piezoelectric Cantilever-Based MEMS Sensor, IEEE Sensors Journal, 17 (2017) 6279-6294.
[31] A. Rahi, Crack mathematical modeling to study the vibration analysis of cracked micro beams based on the MCST, Microsystem Technologies, (2018).
[32] A. Rahi, H. Petoft, Free vibration analysis of multi-cracked micro beams based on Modified Couple Stress Theory, Journal of Theoretical and Applied Vibration and Acoustics, 4 (2018) 205-222.
[33] P. Laura, J. Pombo, E. Susemihl, A note on the vibrations of a clamped-free beam with a mass at the free end, Journal of Sound and Vibration, 37 (1974) 161-168.
[34] J.S. Wu, T.L. Lin, Free vibration analysis of a uniform cantilever beam with point masses by an analytical-and-numerical-combined method, Journal of Sound and Vibration, 136 (1990) 201-213.
[35] M.H. Ghayesh, A. Farajpour, A review on the mechanics of functionally graded nanoscale and microscale structures, International Journal of Engineering Science, 137 (2019) 8-36.
[36] S. S.Rao, Vibration of Continuous Systems, wiley, john wiley and sons, 2007.